Australian Journal of Basic and Applied Sciences, 4(2): 197-207, 2010
ISSN 1991-8178

Element Mobility in Alteration Zones Within Miduk Porphyry Copper Deposit, Shahr – Babak, Kerman, Iran

[1]Mojtaba Mortazavi, [2]Pejman Tahmasebi, [2]Ardeshir Hezarkhani

[1]Department of Mining Engineering, Azad University of Tehran, Tehran, Iran
[1,2.]Department of Mining, Metallurgy and Petroleum Engineering, Amirkabir University, Hafez Ave. No. 424, Tehran, Iran

Abstract: The Miduk porphyry copper deposit is located in SSE central Iran in the elongated NW-trending median mountain range of Kerman Province (85 km northwest of the Sar-Cheshmeh porphyry copper deposit). It is associated with Miocene quartz-diorite to quartz-monzonite which intruded Eocene volcanosedimentary rocks. Copper mineralization was accompanied by both potassic and phyllic alteration. Field observations and petrographic studies demonstrate that emplacement of the Miduk pluton took place in several intrusive pulses, each with associated hydrothermal activity. In this study the investigated alterations were potassic, transition, phyllic and propylitic. For determine the mass transfer volume it was use isocon analysis that explain the changes quantitatively. The result of applying this method is presenting the elements that named enrichment, depletion and immobile. According to this method and the obtained plots, Si, Ti, Al, Ga were relatively immobile during alteration and the mass changes during these process and alteration were approximately near to zero. In potassic alteration zone there is obvious enrichment of K, Ba and depletion of Na, Ca, Mg and Mn. Potassic alteration was associated with a major addition of Cu, as evident from the occurrence of disseminated chalcopyrite and bornite in this zone. In the transition alteration zone, Ca was added, Cu and K were depleted and Na and Mg were relatively unchanged. One of the reasons for this for loss of K is relative to Na, which reflects the replacement of K-feldespar by albite. In phyllic alteration zone, Na, K and Ba were depleted and Cu, Ca and Fe were enriched. The loss of K and Na reflects the sericitization of alkali feldspar (such hydrothermal biotite that formed in potassic alteration). Finally in the propylitic alteration zone Fe and Ba were depleted and Ca, Mg, Na and Cu were enriched. Depletion of Fe was due to the alteration of Fe-rich magmatic amphibole and biotite, by biotite and phengitic muscovite with appreciably lower Fe/Fe+Mg ratio.

Key words: Miduk, Mass transfer, Enrichment, Depletion, Immobile.

INTRODUCTION

Although porphyry copper deposits have been intensively in the Mesozoic-Cenozoic orogenic belts of the American Cordillera and the East Pacific Rim (Niazi and Asoudeh, 1978) their genesis is relatively well understood, few investigation of this style of mineralization have been undertaken in Iran and southern Asia. All known Iranian porphyry copper mineralization are in Cenozoic Sahand-Bazman orogenic belt (Fig. 1). This belt was formed by subduction of the Arabian plate beneath central Iran during the Alpian orogeny (Berberian and King, 1981; Hassanzadeh, 1993) and hosts two major porphyry Cu deposits. The sar-Cheshmeh body is the only one of these currently being mined, and contains 450 million metric tons of sulfide ore with an average grade of 1.13 Cu and ~ 0.03 % Mo (Ulrich and Henric, 2001). The Sungun deposit, which contains 500 million tons of sulfide reserves grading 0.76 % Cu and ~0.01 percentage Mo (National Iranian Industries Copper Company [NICIC], unpubl. Data) is currently being developed. Sar-Cheshmeh, Miduk and a number of economic porphyry copper deposits are all associated with the mid to late Miocene diorite/granodiorite to quartz-monzonite stocks (Hezarkhani, 2008; Hezarkhani and Williams-Jones, 1998). The Miduk porphyry copper system is a quartz diorite-related deposite located 85 km NW of Sar-cheshmeh (Fig. 2). Cores totaling more than 8000 m from 33 diamond drill holes to depths of 300 m have been examined by the NICIC.

Corresponding Author: Pejman Tahmasebi, Department of Mining, Metallurgy and Petroleum Engineering, Amirkabir University, Hafez Ave. No. 424, Tehran, Iran

Many studies of porphyry copper deposits have provided descriptions of minerals present in different alteration zones, and chemical characteristics of fluids associated with alteration episodes (Beane and Bodnar, 1995; Brimhall, 1980; Cartnt,1986). However, there have been only a few attempts to determine the complete evolutionary path of alteration, with corresponding quantification of mass changes in different alteration zones during reaction with hydrothermal fluids (Hezarkhani, 2004).

In this paper, the mass changes of major and minor elements of the Miduk porphyry copper are evaluated quantitatively. The method of Gresens (1967) and, as modified by Grant (1986), is employed to calculate mass changes during alteration. These elements are used to establish bulk mass/volume changes during the different alteration episodes. Mass of the components added to or removed from the rock as a result of interaction with hydrothermal fluids are determined by comparing the corrected analyses for the altered rocks with those of least-altered equivalents. By comparing the results from this study with data available from previous papers, it has been possible to contribute a better understanding of the nature of Iran porphyry copper systems.

Geological Setting of the Miduk Deposit: The Miduk porphyry copper deposit is located on Kuh e La Chah (La Chah Mountain) about 4 km northeast of the village of Miduk and about 45 km by road from Shahr e Babak. Kuh e La Chah is a northfacing U-shaped ridge, 1.2 km in diameter that stands 2700–2850 m above sea level. The deposit lies in a basin confined within the curved ridge (Beane and Bodnar, 1995). Kuh e La Chah and the surrounding area has been the scene of mineral prospecting since ancient time. However, porphyry mineralization was recognized only after discovery of Sar-Cheshmeh in the 1970s. The smaller diorite-type Miduk stock differs from the Sar-Cheshmeh stock in several respects (Beane and Bodnar, 1995). The porphyry complex forms a semi-radial quartz diorite cupola, and is surrounded by intensely biotitized volcanic wall rock. In contrast to Sar Cheshmeh, alkali metasomatism at Miduk is characterized by four different alteration assemblages: potassic, transition (sodic-potassic), phyllic, and propylitic. Albite is the sodic phase. A propylitic alteration zone, characterized by ubiquitous epidote and chlorite mineralization, surrounds the entire complex. La Chah Mountain consists of rock from the lower unit (Razak volcanogenic complex) of the Paleogene sequence intruded by late middle Miocene porphyry dikes. The peculiar morphology is due to intense silicification with relict signs of phyllic alteration concentrated along the ridge. As a result of supergene processes, the rocks are also strongly bleached at the surface. Diamond drill cores to depths of 300 m, however, have provided the opportunity to document multiple intrusions and to identify hypogene alteration-mineralization assemblages (Beane and Bodnar, 1995; Hezarkhani and Williams-Jones, 1998).

The other major phases participating in the alkali metasomatized rocks are quartz + biotite ± K-feldspar + chalcopyrite + pyrite ± magnetite. Anhydrite and molybdenite are rare (Beane and Bodnar, 1995; Hezarkhani, 2008). The alkali metasomatic assemblages have been overprinted by a retrograde phyllic alteration characterized by quartz + sericite + pyrite ± chlorite (in mafic volcanic country rocks). Unlike Sar Cheshmeh, this phyllic alteration at Miduk weakens outward (Hezarkhani, 2008).

Miduk is characterized by four different alteration assemblages: potassic, transition (sodic-potassic), phyllic, and propylitic. Albite is the sodic phase.

A. Alteration and Mineralization:

I) Alteration:

Alteration and related mineralization in the Miduk porphyry copper deposit were investigated by geological mapping, and through detailed studies of the mineralogy, petrography, and chemistry of a large number of drill cores and outcrop samples from various parts of the intrusive (Figs. 2). Four different hypogene alteration assemblages occur in the Miduk deposit: potassic, transition (sodic-potassic), phyllic, and propylitic (Hezarkhani, 2008).

a) Potassic Alteration:

The earliest intense alteration is represented by potassic mineral assemblages developed pervasively and as halos around veins in the deep and central parts of the Miduk intrusive. Potassic alteration is characterized by K-feldspar, irregularly shaped crystals of Mg-enriched biotite, and anhydrite, which is characteristic of alkali metasomatism (Beane and Bodnar, 1995; Hezarkhani, 2008). This alteration displays a close spatial association with mineralization; perhaps as much as 70% of the copper was emplaced during this alteration episode (Hezarkhani, 2008).

c) Propylitic Alteration:

There is a relatively sharp boundary between the propylitic and potassic alteration zones in the deep part of the deposit, but at shallow levels this contact is obscured by later phyllic alteration. The propylitic alteration zone is approximately 400 m thick, characterized by ubiquitous epidote, plagioclase, and chlorite (± pyrite ±

calcite). It is peripheral with respect to the alkali metasomatized zone. Propylitic alteration is pervasive and is represented mainly by chloritization of primary and secondary biotite and groundmass material in rocks peripheral to the central potassic zone. Epidote replaced plagioclase, but this alteration is less pervasive and intense than the chloritization (Hezarkhani, 2008). Microprobe analyses indicate that the chlorite composition corresponds mostly to that of clinochlore and pycnochlorite. Minor minerals associated with propylitic alteration are albite, calcite, sericite, anhydrite (gypsum), and pyrite (Hezarkhani, 2008).

c) Sodic Alteration:

Potassic alteration is overprinted by a large zone of pervasive sodic alteration in the central part of the stock, which grades peripherally into phyllic alteration. End-member sodic alteration typically occurs as pure albite envelopes up to 2 cm thick around B-veins and biotite veinlets. Sodic alteration is characterized by albite replacement of more An-rich plagioclase, and albite rims on orthoclase. Minor sericite with pyrite also partially replaced plagioclase, biotite, and hornblende (Beane and Bodnar, 1995).

A distinguishing characteristic of this type of alteration is the white color of the affected rocks. This change of color from the original grey to white reflects a strong depletion of ferromagnesian minerals like hornblende and biotite.

d) Phyllic Alteration:

The transition from sodic alteration to phyllic alteration is gradual and is marked by an increase in the proportion of muscovite. It is difficult to separate sodic and phyllic alteration because of intense silicification during the latter alteration. Phyllic alteration overprinted alkali metasomatic assemblages.

The phyllic alteration is typically weak within the porphyry complex, and mostly confined to pyrite ± chalcopyrite ± quartz veins except for intervals within ca. 100–250 m where feldspars and mafic silicates are entirely replaced by sericite associated with quartz and pyrite (Beane and Bodnar, 1995; Hezarkhani, 2008).

e) Argillic Alteration:

Feldspar is locally altered to clay down to a depth of 20 m, and the entire rock has been altered to an assemblage of clay minerals, hematite, and quartz. The affected rocks are soft and white. XRD analyses indicate that kaolinite is the dominant phyllosilicate, and that it is accompanied by illite. The shallow alteration is interpreted to represent a supergene blanket over the deposit, and the deeper clay alteration of feldspar may have had the same origin. However, the possibility cannot be excluded that the latter represents an advanced argillic stage of hypogene alteration. Supergene enrichment has developed a blanket several meters thick within the porphyry complex (Beane and Bodnar, 1995; Hezarkhani, 2008). It consists principally of chalcosite. Covellite is present in trivial quantities. The supergene sulfide blanket is overlain by a leached capping layer averaging 50 m in thickness. Oxide ore contains limonite, copper carbonates, and chalcantite as well as turquoise and chrysocolla in places (Beane and Bodnar, 1995; Hezarkhani, 2008).

II) Mineralization:

Hypogene copper mineralization appears to have been introduced during the transition from potassic/sodic to phyllic alteration and mainly during phyllic alteration. The earlier mineralization occurs predominantly as veins with sericitic halos in the potassic zone and the later mineralization as disseminations and veinlets. During potassic alteration, the copper mineralization consisted of chalcopyrite and minor bornite; chalcopyrite was the only copper phase during later hypogene mineralization. Alteration of feldspars and biotite (from potassically altered rocks) to sericite and chlorite was accompanied by an increase in sulfide content outward from the central part of the stock to its margins. Copper mineralization increases from less than 0.20 wt% in the potassic core to a maximum of 1.2 wt% in the phyllic zone and then decreases. The pyrite content is highest (3–10 vol% of the rock) in the quartz-sericite (phyllic) zone. The ratio of pyrite to chalcopyrite in the zone of richest hypogene copper mineralization is as low as 3:1, but toward the margins of the stock the ratio increases to 13:1 (Hezarkhani, 2008). There is an attempt, according to current data sets; sampling has been performance such that they could hole all of these alteration characteristics. Representative samples were examined from the different alteration zones from the deposit as well. Detailed petrographic studies of wall rock, viens, and alteration envelopes were performed on 40 thin sections, 50 polished sections and 45 polished thin sections. Mineral identification and qualitative estimation of mineral abundance were conducted using optical microscopy on polished thin sections and by electronmicroprobe analyses on variety of minerals (Beane and Bodnar, 1995; Hezarkhani, 2008).

Mass Changes During Alteration:

Several methods have been used to calculate mass losses or gains in ore deposits: the volume factor

method of Gresens (1967); the isocon method of Grant (1986); and the immobile element method of MacLean and Kranidiotis (Hezarkhani *et al.,* 1999). In this study, mass gains and losses during alteration were calculated using the method of Grant (1986). In order to avoid errors due to variations inherent in the density of the least-altered rock, a sample from the deepest part of the diorite/granodiorite intrusion was selected and tested by comparing it with the other 'fresh' rocks from the deposit. This sample, a diorite/granodiorite No. TMR32, is very similar compositionally to the other 'fresh' rock and was used to represent the least-altered rock (see figure 3). The diorite/granodiorite contains ~50% by volume of phenocrysts consisting mainly of zoned plagioclase (An_{15-32}), altered hornblende, quartz and biotite and is distinguished from the monzonite or quartz–monzonite by the lack of Kfeldspar phenocrysts. Hornblende was the earliest major mineral to crystallize and forms euhedral to subhedral phenocrysts. Quartz phenocrysts crystallized next and are ubiquitously rounded or embayed, which is a (predicted) consequence of isothermal decompression of a water vapor under saturated magma. Plagioclase phenocrysts (mainly subhedral) formed shortly after the quartz phenocrysts, and biotite phenocrysts (subhedral to anhedral) formed late. The diorite/granodiorite groundmass is finegrained and consists mainly of quartz, plagioclase, and Kfeldspar, with lesser biotite and amphibole.

Apatite, zircon, scheelite, titanite, uraninite and rutile are present in minor to trace amounts. Petrographic examination indicates that even in this sample there was limited alteration of feldspars, hornblende and biotite to muscovite, quartz and oxides. However, this will not greatly affect interpretations of the alteration reactions, which are based on comparisons between different alteration zones.

The isocon approach of Grant (1986) is mathematically similar to that of Gresens (1967), but differs in the graphical representation of the data. In Gresens' method, the components that are likely to have been immobile during alteration can be used to identify any volume change, which may have taken place. If it is assumed that volume change is a factor common to the behavior of all components, it is possible to calculate gains or losses of the other components. Mass gains and losses are calculated using the following relationship:

$$X_n = [F_v(S^b/S^a)C_n^b - C_n^a] \times 100 \quad (1)$$

where, X_n is the mass gain or loss for component n, F_v is the volume factor, S^b is the specific gravity of the altered sample, S^a is the specific gravity of the unaltered (original) sample, C_n^b is the concentration of component n in the altered sample, and C_n^a is the concentration of component n in the unaltered (original) sample. In the isocon method of Grant (1986), Eq. (1) is reformulated as: where M^b/M^a is the mass ratio between the altered sample and the unaltered sample.

This ratio is calculated by plotting the concentration of components in the altered rock (e.g. X-axis) versus those in the unaltered sample (e.g. Y-axis). The components that are immobile will fall on a line of slope M^b/M^a; referred to as the isocon.

$$DX_n = 100(M^b/M^a)X_n^b - X_n^a \quad (2)$$

Components that lie above the isocon have been added while those which are below the line have been lost during the alteration. The slope of the isocon (mass factor) can be determined graphically, and is used to calculate the mass gains and losses of the remaining components by applying Eq. (2)

Mass Changes:

A. Potassic Alteration:

Comparison of sample TMR11 (representative of the potassic zone) with least-altered sample TMR32 shows that the immobile elements, Si, Ti, Al and Ga plot close to or on a line of constant mass with a slope of 1.0 (Fig. 4).

However, the elements Nb which is generally considered to be geochemically immobile, plot off the line, possibly due to a nugget effect. As expected from the mineral assemblage in the potassic alteration zone, K and Ba are enriched in sample TMR11 and copper, as expected, is strongly enriched. By contrast Na is depleted, as are Mg, Ca and Mo. Mass changes associated with potassic alteration are presented numerically in Table 2. Most calculated volume factors (VF) lie between 0.98 and 1.03, (Table 3, Fig. 4) indicating that there was essentially no volume change.

B. Transition Alteration:

The transition alteration zone is transitional between the potassic alteration zone and the phyllic alteration

zone, but is clearly superimposed on the potassic alteration zone. In order to determine mass changes associated with this alteration, the reference for comparison was therefore a potassically altered rock (TMR10).

Comparison of a representative sample of rock that has undergone transition alteration (TMR2) with potassically altered rock (TMR10) shows that TiO_2, Al_2O_3, Nb, U, Mn and Ga plot close to or on a line of constant mass with a slope of approximate 1.0 (Table 2, Fig. 5). Most calculated volume factors also lie between 0.97 and 1.01, indicating that there was essentially no volume change. The mass changes of major and trace elements are plotted in Fig. 5 (also see Table 2).

Relative to potassically altered rocks Cu, K and Ca were depleted and Na and Mg were added in the transition zone. Absolute mass gains and losses are evaluated quantitatively in Table 3.

C. Phyllic Alteration:

The phyllic alteration zone is characterized by the presence of large proportions of sericite and pyrite and the near absence of biotite and K-feldspar. Phyllic alteration has strongly overprinted earlier potassic alteration. Comparison of potassically altered sample TMR5 and representative sample of TMR14 for phyllic alteration shows that the immobile elements Al, Si, Mn, Nb,Ga and Ti plot close to or on a line (Fig. 6) of constant mass with a slope of 1.0. However, Zr, which is

Typically immobile, plots off the line, due possibly as discussed earlier, to a nugget effect. Most calculated volume factors lie between 0.98 and 1.04, indicating that there was only minor volume change. The most important mass changes in the phyllic alteration zone relative to potassically altered rock are depletion of Na and Ba, and addition of Ca, Mn, and Fe_2O_3 and Cu.

D.propylitic Alteration:

This alteration covered the former alteration from its external section. it is limited from up to phyllic In the near of potassic alteration or toward the system center, the epidote and cholorite have been increased. But toward the external section, the epidote has been decreased and despite of it the albite, calcite and montmorilonite have been replaced. Comparison of a representative rock sample that has undergone phyllic alteration (TMR1) with propylitic altered rock (TMR31) shows that TiO_2, Al_2O_3, Nb, K_2O and Ga plot close to or on a line of constant mass with a slope of approximate 1.0 (Table 2, Fig. 7). Most calculated volume factors also lie between 0.99 and 1.02, indicating that there was essentially no volume change. The mass changes of major and trace elements are plotted in Fig. 7 (also see Table 2). Relative to phyllicaly altered rocks Cu, K, Na and Ca were depleted and Ba, Zr and Fe_2O_3 were added in the propylitic zone. Depletion of Fe was due to the alteration of Fe-rich magmatic amphibole and biotite, by biotite and phengitic muscovite with appreciably lower Fe/ Fe +Mg ratio. Absolute mass gains and losses are evaluated quantitatively in Table 3.

Discussion:

Based on the studies of fluid evolution in the Miduk deposit Hezarkhani, (2008). The first hydrothermal fluid caused potassic alteration and Cu ± Mo (very rare Mo) mineralization. This fluid was characterized by high temperatures and moderate to high salinities, and was probably magmatically derived were at temperatures ranging from 370 to 530°C, and boiled episodically. The second hydrothermal fluid was formed mainly by the mixing of magmatic fluid, at moderate to low temperatures (up to 450°C), with a predominantly meteoric fluid and also boiled.

This fluid was responsible for the sodic and sericitic alteration zones in the upper portion of the stock. The third hydrothermal fluid consisted of low temperature, low- to moderate-salinity (1 to 20 wt% NaCl equiv.), and oxidized meteoric water, which was responsible for peripheral propylitic alteration in a zone outside the core of potassically altered rock, and argillic alteration in regions where it penetrated into the system. This addition of external fluids increased Na/K ratios in the progressively heated fluids, and caused the remobilization of previously precipitated copper sulfides through acidification and oxidation, and redeposition in highly fractured zones in the apical part of the intrusion. This is evident from the occurrence of chalcopyrite as overgrowths on earlier grains of chalcopyrite. Final supergene enrichment of copper minerals was very limited, and consists of a thin blanket containing covellite, chalcocite digenite and turquoise located below an intensely altered cap Hezarkhani, (2008). At all stages in the evolution of the Miduk hydrothermal system, alteration appears to have taken place with no appreciable change in volume as shown by the fact that the volume factors (VF) calculated earlier are close to unity. In the potassic alteration zone, the principal chemical changes were the enrichment of K, Cu and Ba, and the depletion of Na, Ca, Mg and Mn. Mineralogically, these changes were accommodated by crystallization of K-feldspar and biotite at the expense of plagioclase and amphibole (Hezarkhani *et al.,* 1999).. The replacement of plagioclase and amphibole by K-feldspar and biotite, respectively, served to add K and remove Ca and Na. The changes in K and Na are

consistent with fluid inclusion data (Hezarkhani *et al.,* 1999). which suggest comparably high K/Na ratio and low concentrations of cations of other major elements. Barite was not found in the Miduk deposit, and the only minerals that could accommodate Ba are K-feldspar and mica, which formed in potassically altered rocks. Copper was added to potassically altered rocks in significant amount as might be expected from the dissemination of chalcopyrite and bornite in this zone.

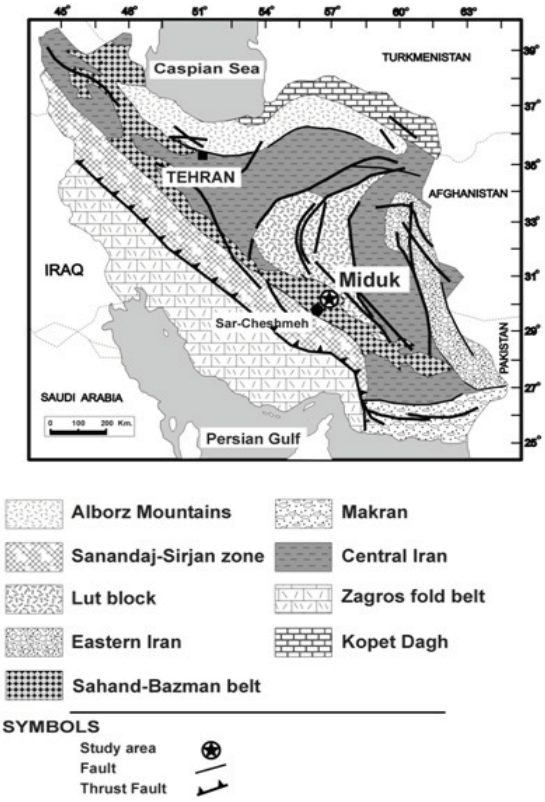

Fig. 1: Geological map of Iran showing major lithotectonic units and the Midul deposit situation Hezarkhani, (2002).

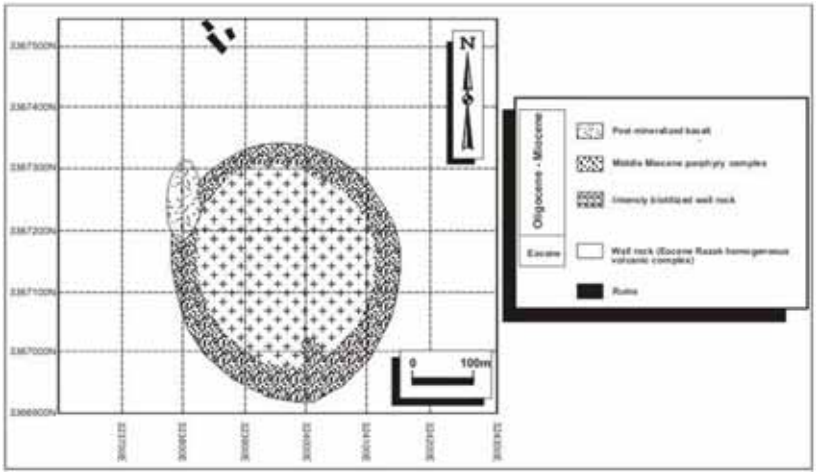

Fig. 2: Detailed geological map of the Miduk area showing the distribution of different igneous suites (modified from (Beaneand Bodnar, 1995).

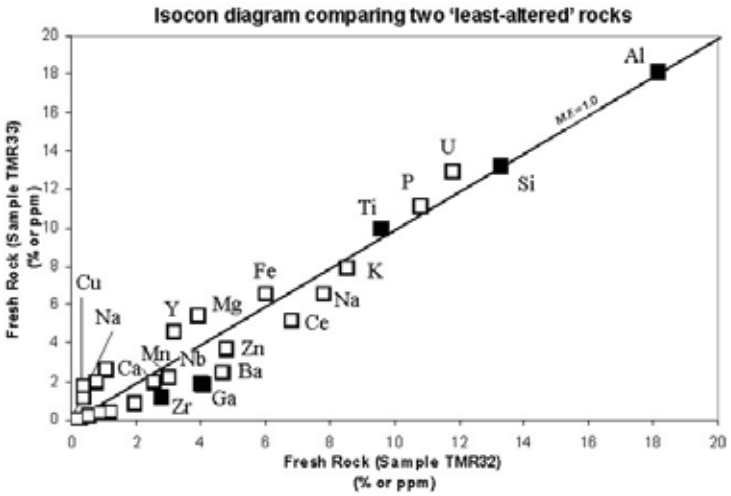

Fig. 3: Isocon diagram comparing two 'least-altered' rocks. Almost all major oxides fall on or near a line.

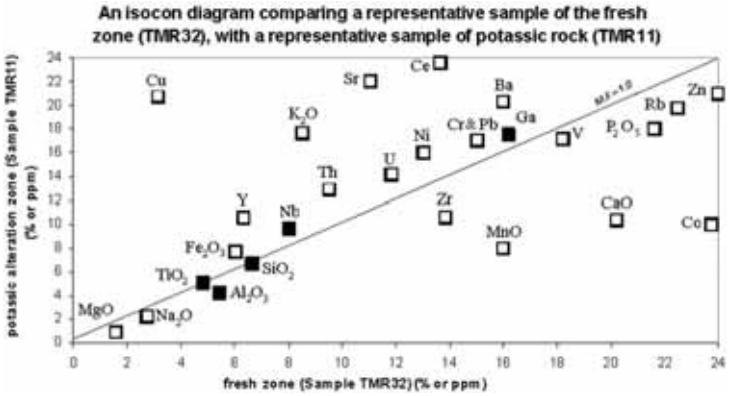

Fig. 4: An isocon diagram comparing a representative sample of the potassic alteration zone (TMR11), with a representative sample of least-altered rock (TMR32). The dashed line (isocon) is drawn for the largest number of potentially immobile elements (solid squares). The best constraints on mass changes during potassic alteration are given by TiO2, Al2O3, SiO2, Nb and Ga. Only those elements on the isocon, and those present in appreciable concentrations have been labeled. The inset histogram shows the distribution of mass factors calculated for each element.

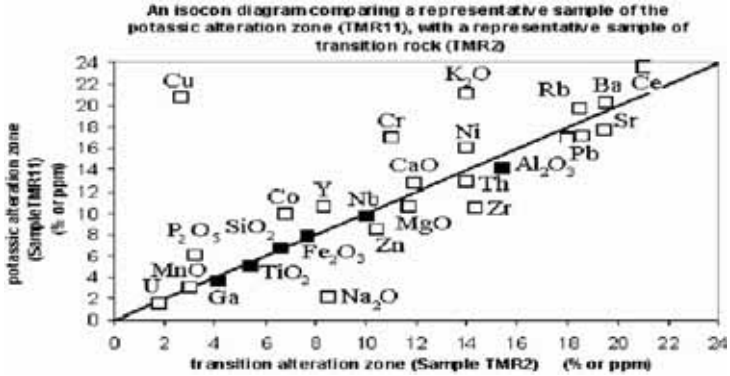

Fig. 5: Isocon diagram comparing the composition of a representative sample of an altered rock from the transition zone with that of a representative potassically altered rock. See text and caption of Fig. 4 for details.

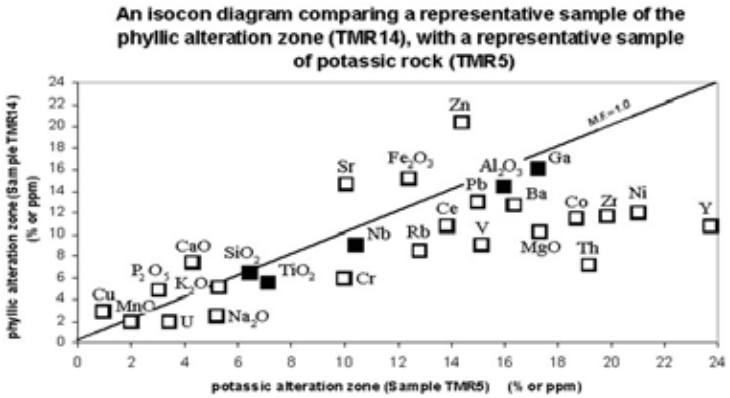

Fig. 6: Isocon diagram comparing the composition of a representative sample of a representative phyllically altered rock with that of a potassically altered rock. See text and caption of Fig. 4 for details.

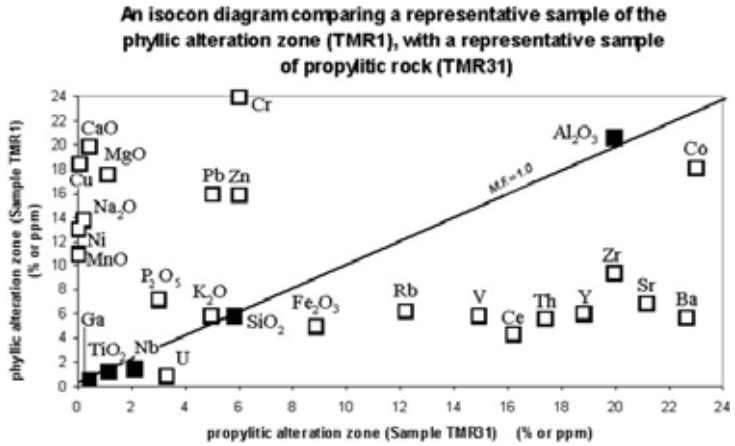

Fig. 7: Isocon diagram comparing the composition of a representative sample of a representative phyllically altered rock with that of a propyliticlly altered rock. See text and caption of Fig. 4 for details.

Conclusion:

Isocon analysis provides a simple and effective means of quantitatively evaluating chemical gains and losses in mass transfer. This method has been applied to a wide range of geological processes, from hydrothermal alteration to formation of silcretes. Sampling the altered rock is generally less problematic, even if the alteration is zoned. Given zonation or general heterogeneity of the rocks, judicious sampling and averaging of samples is necessary. The choice of immobile species can be determined from the clustering of

C_i^A / C_i^O or a best fit of data forming a linear array through the origin on an isocon diagram (the graphical

equivalent) that according to applying this method, Al, Ti and Ga were relatively immobile during the different alterations. In the potassic alteration zone, the changes in major elements were enrichment in K, Ba, and Cu, and depletion in Na, Ca, Mn and Mg. In the transition alteration zone, Ca was added, Na and Mn were relatively unchanged, and K and Cu were depleted. In the propylitic alteration zone, Ca, Mg, Na and Cu were added, and Ba and Fe were depleted. The reasons for these changes were mentioned earlier that proved the obtained results from this method. According to this study it is clear that by applying this method, researchers could be able to determine the enrichment of each zone rather to specific element and also separate the economic mining boundary. Other approaches by applying this method are investigation of alteration process in the mining confine and conduct that to mineralization zones and determine the typical elements of each alteration that could be applied to distinguish of alteration boundary and finally with all of this advantages, this method could be cause to decreasing of exploration and drilling costs and determine of alteration type by exposed altered rocks.

Table 1: Variations in major and trace element mass changes in the fresh rocks.

type	Fresh Rocks			Molecular proportion			Range	Average
no.	1	2	3	1	2	3		
sample	TMR32	TMR33	TMR34	TMR32	TMR33	TMR34		
g/100 g								
SiO_2	66.31	66.14	65.20	74.47	74.64	65.22	9.42	71.44
AI_2O_3	18.12	18.17	0.54	15.31	15.42	13.62	1.81	14.78
Fe_2O_3	6.02	6.56	15.73	3.98	4.36	9.27	5.29	5.87
MgO	1.56	2.16	4.08	0.66	0.92	1.54	0.88	1.04
MnO	0.04	0.03	0.08	0.04	0.03	0.07	0.04	0.04
TiO_2	0.48	0.50	1.74	0.80	0.84	0.73	0.11	0.79
CaO	2.54	1.97	3.83	3.06	2.38	4.10	1.72	3.18
Na_2O	0.27	0.08	3.75	0.29	0.09	3.64	3.55	1.34
K_2O	1.70	1.59	2.73	1.22	1.14	1.74	0.60	1.37
P_2O_5	0.36	0.37	0.18	0.17	0.18	0.08	0.10	0.14
g/1000 kg								
Cu	30.00	50.00	25.00	78.04	91.88	88.01	13.84	85.98
Ba	320.00	182.00	203.00	3.63	0.79	1.46	2.84	1.96
Ce	27.30	20.60	25.20	0.30	0.09	0.18	0.22	0.19
Co	23.70	8.60	10.16	0.63	0.09	0.17	0.54	0.29
Cr	150.00	390.00	236.00	4.50	4.49	4.47	0.03	4.48
Ga	16.20	7.30	10.20	0.36	0.06	0.14	0.30	0.19
Nb	8.00	3.80	5.00	0.13	0.02	0.05	0.11	0.07
Ni	13.00	11.00	12.00	0.35	0.11	0.20	0.23	0.22
Pb	15.00	37.00	23.00	0.27	0.26	0.26	0.01	0.27
Rb	74.90	35.70	56.20	1.37	0.25	0.65	1.12	0.75
Sr	221.00	99.90	120.30	3.93	0.68	1.35	3.25	1.99
Th	9.53	3.59	6.25	0.06	0.01	0.03	0.05	0.03
U	1.18	1.30	12.30	0.01	0.00	0.05	0.05	0.02
V	91.00	40.00	63.00	2.79	0.47	1.22	2.32	1.49
Y	6.30	9.20	7.30	0.11	0.06	0.08	0.05	0.08
Zn	48.00	37.00	41.20	1.14	0.34	0.62	0.81	0.70
Zr	138.50	60.30	98.30	2.37	0.40	1.06	1.97	1.27

Table 2: Major and trace element mass changes at the Miduk deposit (the previously altered rock is the original rock for the next alteration stage except for phyllic alteration which is superimposed on potassic alteration).

type	Potassic Alteration			Molecular proportion			Mass changes in potassic alteration zone			Range	Average	M.D[1]	δ^2
no.	1	2	3	1	2	3	1	2	3				
sample	TMR5	TMR10	TMR11	TMR5	TMR10	TMR11	TMR5	TMR10	TMR11				
g/100 g													
SiO_2	64.35	63.21	66.74	74.69	76.20	76.70	0.22	1.73	2.23	64.35	63.21	66.74	0.49
AI_2O_3	15.95	15.81	14.14	13.91	14.32	12.21	-1.40	-0.99	-3.10	15.95	15.81	14.14	0.53
Fe_2O_3	6.20	6.34	7.76	4.24	4.50	5.26	0.26	0.52	1.27	6.20	6.34	7.76	0.25
MgO	1.73	0.44	0.88	0.76	0.20	0.38	0.10	-0.46	-0.28	1.73	0.44	0.88	0.13
MnO	0.02	0.02	0.02	0.02	0.02	0.02	-0.02	-0.02	-0.02	0.02	0.02	0.02	0.00
TiO_2	0.71	0.58	0.51	1.23	1.04	0.87	0.42	0.24	0.07	0.71	0.58	0.51	0.08
CaO	0.43	0.44	1.28	0.53	0.57	1.58	-2.52	-2.49	-1.48	0.43	0.44	1.28	0.28
Na_2O	0.52	0.89	0.22	0.59	1.04	0.25	0.29	0.75	-0.05	0.52	0.89	0.22	0.19
K_2O	5.25	2.58	3.54	3.89	1.98	2.60	2.67	0.77	1.38	5.25	2.58	3.54	0.46
P_2O_5	0.31	0.24	0.30	0.15	0.12	0.15	-0.02	-0.05	-0.03	0.31	0.24	0.30	0.01
g/1000 kg													
Cu	5200.0	2900.00	20800.00	81.83	456.30	327.30	5175.0	19575.00	20775.0	5200.00	2900.00	20800	409
Ba	544.00	117.50	406.00	3.96	0.86	2.96	341.00	207.00	203.00	544.00	117.50	406.0	37.0
Ce	69.20	44.50	47.20	0.49	0.32	0.34	44.00	19.00	22.00	69.20	44.50	47.20	6.40
Co	18.70	81.00	10.00	0.32	1.37	0.17	8.50	-0.70	-0.20	18.70	81.00	10.00	2.40
Cr	100.00	100.00	170.00	1.92	1.92	3.27	-136.00	-156.00	-66.00	100.00	100.00	170.0	22.3
Ga	15.70	19.60	17.60	0.23	0.28	0.25	5.50	6.60	7.40	15.70	19.60	17.60	0.40
Nb	10.40	10.20	9.70	0.11	0.11	0.10	5.40	5.40	4.70	10.40	10.20	9.70	0.20
Ni	21.00	14.00	16.00	0.36	0.24	0.27	9.00	-1.00	4.00	21.00	14.00	16.00	2.40
Pb	15.00	13.00	17.00	0.07	0.06	0.08	-8.00	-3.00	-6.00	15.00	13.00	17.00	1.20
Rb	128.00	75.60	65.90	1.50	0.88	0.77	71.80	21.50	9.70	128.00	75.60	65.90	15.5
Sr	100.50	121.00	441.00	1.15	1.38	5.03	-19.80	268.70	320.70	100.50	121.00	441.0	86.5
Th	19.15	16.60	12.85	0.08	0.07	0.06	12.90	5.20	6.60	19.15	16.60	12.85	1.90
U	3.43	1.64	1.42	0.01	0.01	0.01	-8.90	-10.90	-10.90	3.43	1.64	1.42	0.60
V	151.00	81.00	86.00	2.96	1.59	1.69	88.00	10.00	23.00	151.00	81.00	86.00	19.7
Y	23.70	11.50	10.60	0.27	0.13	0.12	16.40	1.70	3.30	23.70	11.50	10.60	3.80
Zn	36.00	59.00	42.00	0.55	0.90	0.64	-5.20	7.80	0.80	36.00	59.00	42.00	3.10
Zr	198.50	126.00	105.50	2.18	1.38	1.16	100.20	21.70	7.20	198.50	126.00	105.5	23.6
g/100 g													
SiO_2	62.34	59.81	65.97	73.25	71.24	75.90	-1.44	-3.45	1.21	4.66	-1.23	1.63	1.10
AI_2O_3	16.93	16.17	15.41	14.96	14.49	13.34	1.06	0.58	-0.57	1.63	0.35	0.62	0.39
Fe_2O_3	7.81	8.71	7.66	5.41	6.11	5.19	1.17	1.87	0.95	0.92	1.33	0.36	0.23
MgO	1.68	3.61	0.97	0.74	1.62	0.42	-0.01	0.86	-0.34	1.20	0.17	0.46	0.29
MnO	0.02	0.04	0.02	0.02	0.04	0.02	0.00	0.02	0.00	0.02	0.01	0.01	0.01
TiO_2	1.05	1.06	0.54	1.84	1.88	0.93	0.61	0.65	-0.30	0.96	0.32	0.42	0.25
CaO	0.12	0.74	1.19	0.15	0.94	1.47	-0.38	0.41	0.93	1.32	0.32	0.47	0.31
Na_2O	0.09	0.13	0.85	0.10	0.15	0.95	-0.48	-0.44	0.36	0.85	-0.18	0.37	0.22
K_2O	4.55	4.40	2.33	3.41	3.34	1.71	-0.48	-0.54	-2.18	1.70	-1.07	0.74	0.45
P_2O_5	0.23	0.36	0.16	0.11	0.18	0.08	-0.04	0.03	-0.07	0.10	-0.03	0.04	0.02

Table 2: Continue

g/1000kg													
Cu	7300.00	9600.00	2600.00	114.87	465.77	40.91	-13500.	8800.00	-18200.0	7300.00	9600.00	2600.00	6799
Ba	347.00	270.00	391.00	2.53	1.97	2.85	-59.00	-136.00	-15.00	347.00	270.00	391.00	28.9
Ce	52.50	51.80	42.00	0.37	0.37	0.30	5.30	4.60	-5.20	52.50	51.80	42.00	2.8
Co	19.80	11.80	6.80	0.34	0.20	0.12	9.80	1.80	-3.20	19.80	11.80	6.80	3.10
Cr	140.00	130.00	110.00	2.69	2.50	2.12	-30.00	-40.00	-60.00	140.00	130.00	110.00	7.20
Ga	16.20	16.20	20.60	0.23	0.23	0.30	-1.40	-1.40	3.00	16.20	16.20	20.60	1.20
Nb	10.20	9.30	10.00	0.11	0.10	0.11	0.50	-0.40	0.30	10.20	9.30	10.00	0.20
Ni	28.00	22.00	14.00	0.48	0.37	0.24	12.00	6.00	-2.00	28.00	22.00	14.00	3.30
Pb	104.00	13.00	18.00	0.50	0.06	0.09	87.00	-4.00	1.00	104.00	13.00	18.00	24.1
Rb	103.00	131.50	61.60	1.21	1.54	0.72	37.10	65.60	-4.30	103.00	131.50	61.60	16.6
Sr	238.00	163.50	486.00	2.72	1.87	5.55	-203.00	-277.50	45.00	238.00	163.50	486.00	79.6
Th	3.54	4.65	14.00	0.02	0.02	0.06	-9.30	-8.20	1.20	3.54	4.65	14.00	2.70
U	2.08	1.80	1.82	0.01	0.01	0.01	0.70	0.40	0.40	2.08	1.80	1.82	0.10
V	180.00	152.00	93.00	3.53	2.98	1.83	94.00	66.00	7.00	180.00	152.00	93.00	20.9
Y	30.60	18.40	8.30	0.34	0.21	0.09	20.00	7.80	-2.30	30.60	18.40	8.30	5.30
Zn	42.00	77.00	52.00	0.64	1.18	0.80	0.00	35.00	10.00	42.00	77.00	52.00	8.50
Zr	164.50	161.00	143.50	1.80	1.76	1.57	59.00	55.50	38.00	164.50	161.00	143.50	5.30
g/100 g													
SiO_2	58.00	64.15	68.12	70.32	75.27	76.25	-4.36	0.58	1.56	5.92	-1.89	2.80	1.64
AL_2O_3	19.96	14.47	14.73	18.21	12.77	12.40	4.30	-1.14	-1.51	5.80	0.55	2.50	1.53
Fe_2O_3	8.88	7.57	3.67	6.35	5.23	2.42	2.10	0.99	-1.82	3.92	0.43	1.50	0.95
MgO	0.11	1.03	1.49	0.05	0.45	0.63	-0.71	-0.30	-0.13	0.58	-0.38	0.22	0.14
MnO	0.00	0.02	0.02	0.00	0.02	0.02	-0.02	0.00	0.00	0.02	-0.01	0.01	0.01
TiO_2	0.56	0.55	0.59	1.01	0.96	0.98	-0.22	-0.27	-0.24	0.05	-0.24	0.02	0.01
CaO	0.09	0.74	0.50	0.12	0.93	0.60	-0.42	0.40	0.06	0.81	0.01	0.29	0.19
Na_2O	0.02	0.25	3.44	0.02	0.28	3.73	-0.56	-0.30	3.15	3.71	0.76	1.59	0.98
K_2O	4.94	5.14	4.00	3.82	3.85	2.86	-0.07	-0.04	-1.03	0.99	-0.38	0.43	0.27
P_2O_5	0.20	0.46	0.23	0.10	0.23	0.11	-0.05	0.08	-0.04	0.13	-0.01	0.05	0.03
g/1000 kg													
Cu	1300.0	3760.00	18200.00	20.50	591.7	286.4	-6000.0	30300.0	10900.0	36300	11733.00	12377.	8562
Ba	1130.0	423.00	488.00	8.20	3.10	3.60	783.00	76.00	141.00	707.00	333.30	299.80	184.2
Ce	80.90	53.80	55.90	0.60	0.40	0.40	28.40	1.30	3.40	27.10	11.00	11.60	7.10
Co	23.00	11.50	9.20	0.40	0.20	0.20	3.20	-8.30	-10.60	13.80	-5.20	5.60	3.50
Cr	60.00	60.00	130.00	1.20	1.20	2.50	-80.00	-80.00	-10.00	70.00	-56.70	31.10	19.10
Ga	187.00	14.60	16.60	2.70	0.20	0.20	170.80	-1.60	0.40	172.40	56.50	76.20	46.70
Nb	10.40	9.00	10.60	0.10	0.10	0.10	0.20	-1.20	0.40	1.60	-0.20	0.70	0.40
Ni	0.00	12.00	14.00	0.00	0.20	0.20	-28.00	-16.00	-14.00	14.00	-19.30	5.80	3.60
Pb	5.00	13.00	23.00	0.00	0.10	0.10	-99.00	-91.00	-81.00	18.00	-90.30	6.20	4.30
Rb	122.00	85.40	94.10	1.40	1.00	1.10	19.00	-17.60	-8.90	36.60	-2.50	14.30	9.00
Sr	302.00	147.00	286.00	3.40	1.70	3.30	64.00	-91.00	48.00	155.00	7.00	65.30	40.20
Th	17.40	7.21	11.00	0.10	0.00	0.00	13.90	3.70	7.50	10.19	8.30	3.70	2.40
U	3.27	1.98	2.15	0.00	0.00	0.00	1.20	-0.10	0.10	1.29	0.40	0.50	0.30
V	149.00	90.00	98.00	2.90	1.80	1.90	-31.00	-90.00	-82.00	59.00	-67.70	24.40	15.10
Y	18.80	10.80	10.40	0.20	0.10	0.10	-11.80	-19.80	-20.20	8.40	-17.30	3.60	2.20
Zn	20.00	51.00	64.00	0.30	0.80	1.00	-22.00	9.00	22.00	44.00	3.00	16.70	10.70
Zr	199.50	117.00	119.00	2.20	1.30	1.30	35.00	-47.50	-45.50	82.50	-19.30	36.20	22.20
g/100 g													
SiO_2	58.16	58.31	57.86	66.25	68.93	67.82	-4.07	-1.40	-2.51	2.67	-2.73	0.97	0.63
AL_2O_3	20.59	22.14	21.98	17.64	19.69	19.38	-0.56	1.48	1.17	2.04	0.70	0.84	0.52
Fe_2O_3	4.99	6.56	6.31	3.35	4.57	4.36	-3.00	-1.78	-1.99	1.22	-2.25	0.50	0.31
MgO	1.75	2.12	2.72	0.75	0.94	1.20	0.70	0.89	1.15	0.45	0.91	0.16	0.11
MnO	0.11	0.17	0.26	0.11	0.17	0.26	0.11	0.17	0.26	0.15	0.18	0.05	0.04
TiO_2	0.64	0.60	0.63	1.09	1.06	1.10	0.07	0.05	0.09	0.04	0.07	0.02	0.01
CaO	3.98	0.47	1.08	4.86	0.60	1.36	4.74	0.48	1.24	4.26	2.15	1.72	1.07
Na_2O	1.37	0.62	0.77	1.51	0.71	0.87	1.49	0.69	0.85	0.80	1.01	0.32	0.20
K_2O	5.79	4.15	4.57	4.21	3.13	3.42	0.39	-0.69	-0.40	1.08	-0.24	0.42	0.26
P_2O_5	0.48	0.42	0.48	0.23	0.21	0.24	0.13	0.11	0.14	0.03	0.12	0.01	0.01
g/1000 kg													
Cu	2600.00	1400.00	1100.00	40.91	22.03	17.31	-35000	-36200	-36500	1500.00	-35900.0	600.00	374.20
Ba	283.00	467.00	3090.00	2.06	3.40	22.50	-140.00	44.00	2667.00	2807.00	857.00	1206.70	740.20
Ce	21.80	38.50	80.10	0.16	0.27	0.57	-32.00	-15.30	26.30	58.30	-7.00	22.20	14.20
Co	18.10	7.00	15.20	0.31	0.12	0.26	6.60	-4.50	3.70	11.10	1.90	4.30	2.70
Cr	240.00	70.00	20.00	4.62	1.35	0.38	180.00	10.00	-40.00	220.00	50.00	86.70	54.40
Ga	13.40	18.10	16.60	0.19	0.26	0.24	-1.20	3.50	2.00	4.70	1.40	1.80	1.10
Nb	7.40	9.20	11.00	0.08	0.10	0.12	-1.60	0.20	2.00	3.60	0.20	1.20	0.80
Ni	13.00	10.00	8.00	0.22	0.17	0.14	1.00	-2.00	-4.00	5.00	-1.70	1.80	1.20
Pb	16.00	20.00	28.00	0.08	0.10	0.14	3.00	7.00	15.00	12.00	8.30	4.40	2.90
Rb	62.30	120.50	192.50	0.73	1.41	2.25	-23.10	35.10	107.10	130.20	39.70	44.90	30.70
Sr	97.80	251.00	716.00	1.12	2.86	8.17	-49.20	104.00	569.00	618.20	207.90	240.70	151.80
Th	5.61	11.20	20.50	0.02	0.05	0.09	-1.60	4.00	13.30	14.89	5.20	5.40	3.50
U	0.84	1.15	4.66	0.00	0.00	0.02	-1.10	-0.80	2.70	3.82	0.20	1.60	1.00
V	58.00	78.00	162.00	1.14	1.53	3.18	-32.00	-12.00	72.00	104.00	9.30	41.80	26.00
Y	6.00	9.30	32.80	0.07	0.10	0.37	-4.80	-1.50	22.00	26.80	5.20	11.20	6.90
Zn	53.00	44.00	259.00	0.81	0.67	3.96	2.00	-7.00	208.00	215.00	67.70	93.60	57.30
Zr	94.50	123.00	208.00	1.04	1.35	2.28	-22.50	6.00	91.00	113.50	24.80	44.10	27.80

Mass transfers are calculated, adjusting for total mass change, using the method explained in the text. Total Fe as Fe_2O_3. $MD^{(1)}$ = measures of dispersion. $\delta^{(2)}$ = standard deviation.

Table 3: Element immobility, mass factor (MF) and volume factor (VF) calculations based on the Isocon method [5]. Sample 30-138 has been chosen as the precursor.

Sample #	Alteration	Relatively Immobile Elements	M.F.	V.F	Average M.F.	Average V.F
TMR3		Ti, Al, Ga, Si, Zn, Rb, Pb	1.02	1.01		
TMR5		Si, Al, Ti, Pb, Fe, Ga, Nb	1.00	1.01		
TMR9		Si, Al, Nb,Ti, Y, Ga, Pb	1.01	0.99		
TMR10		Si,Al, Fe, Ti, Nb, Ni, U,Ga	1.00	1.03		
TMR11	Potassic	Si, Al, Na, Ti, Ga, Fe,V	1.01	1.00	1.01	1.01
TMR13		Ti, Al, Ni, Si, Zn, Ga, Nb, Rb	1.02	1.01		
TMR19		Th, Al, Ti, Si, Ga, Ni, P	1.00	1.02		

Table 3: Continue

TMR20		Si, Al, Ga, Nb, P, Pb, Zr, P	1.01	1.01		
TMR2		Al, Ga, Mn, Rb, Nb, U, P	1.01	1.01		
TMR6	Transition	U, Pb, P, Si, Al, Nb	1.00	0.97	1.01	0.98
TMR16		Ni, Ti, Mn, Al, Ga, Si, U	1.02	0.97		
TMR1		Si, Al, Mn, K, Ga, Nb, Ti, Nb	1.02	1.01		
TMR7		Al, Fe, Si, Ga, Ti, Th	1.00	1.00	1.02	1.01
TMR14	Phyllic	Si, K, Al, Ga, Ti, Mn	1.01	1.02		
TMR15		Si, Al, Mg, Mn, Ti, Ga, Nb	1.03	0.99		
TMR31		Ti, Nb, Si, K, Al	1.00	1.02		
TMR34	propylitic	Ti, Si, Rb, Cr, Al, Nb	1.01	1.01	1.01	1.01
TMR35		Si, Ti, K, Ce, Zr, Al, Nb	1.01	0.99		

REFERENCE

Beane, R.E. and R.J. Bodnar, 1995. Hydrotherma; fluids and hydrothermal alteration in porphyry copper deposits. In Pierce, F.W. and Bohm, J.G., Porphyry copper deposit of American Cordillera. Arizona Geological Society Digest 20, Tucson, Az, pp: 83-93.

Berberian, M., G.C. King, 1981. Towards a paleogeography and tectonic evolution of Iran. Canadian Journal of Earth Sciences, 18: 210-265.

Brimhall, G.H., 1980. Deep hypogene oxidation of porphyry copper potassium silicate protore at Butte, Montana: a theoretical evaluation of the copper remobilization hypothesis. Economic Geology, 75: 384-409.

Carten, R.B., 1986. Sodium calcium metasomatism: chemical, temporal, and spatial relationships at the Yerington, Nevada, porphyry copper deposit. Economic Geology, 81: 1495-1519.

Grant, J.A., 1986. The isocon diagram—a simple solution to Gresens' equation for metasomatic. Economic Geology, 81: 1976-1982.

Gresens, R.L., 1967. Composition–volume relationships of metasomatism. Chemical Geology, 2: 47-55.

Hassanzadeh, J., 1993. Metalogenic and tectonomagmatic events in SE sector of the Cenozoic activecontinental marfin of central Iran (Shahre-Babak, Kerman Province): Unpubl. Ph.D. thesis, University of California, Los Angeles, pp: 204.

Hezarkhani, A., 2002. Mass changes during hydrothermal alteration/mineralization in a porphyry copper deposit, eastern Sungun, northwestern Iran, Journal of Asian Earth Sciences.

Hezarkhani, A., 2008. Hydrothermal Evolution of the Miduk Porphyry Copper System, Kerman, Iran: A Fluid Inclusion Investigation. International Geology Review, 50: 665-684.

Hezarkhani, A., A.E. Williams-Jones, 1998. Controls of alteration and mineralization in the Sungun porphyry copper deposit, Iran: evidence from fluid inclusions and stable isotopes. Economic Geology, 93: 651-670.

Hezarkhani, A., A.E. Williams-Jones, C.H. Gammons, 1999. Factors controlling copper solubility and chalcopyrite deposition in the Sungun porphyry copper deposit, Iran. Mineralium deposita, 34: 770-783.

Niazi, M. and I. Asoudeh, 1978. The depth of seismicity in the Kermanshah region of the Zagros Mountains (Iran): Earth and Planetary Science Letters, 40: 270-274.

Ulrich, T., C. Henric, 2001. Geology and alteration geochemistry of the porphyry Cu-Au deposit at Bajo de Ia Alumbrera, Argentina. Economic Geology, 96: 1719-1742.